Effect of plastic deformation on the evolution of wear and local stress fields in fretting

Zupan Hu[a], Wei Lu[a], M.D. Thouless[a,b], J.R. Barber[a,*]

[a] Department of Mechanical Engineering, University of Michigan, Ann Arbor, MI 48109-2125, USA
[b] Department of Materials Science & Engineering, University of Michigan, Ann Arbor, MI 48109-2136, USA

A B S T R A C T

During fretting, the removal of material by wear leads to an increase of contact stress in the stick zone. If elastic behavior is assumed, the boundary between stick and slip zones does not move, wear eventually ceases, and a mode-I singularity of contact pressure is predicted after infinitely many cycles.

For real materials, the development of singular stresses must be limited by plastic deformation. Here we investigate the effect of plasticity on fretting wear, using a finite-element model. We find that the principal effect of plasticity is to allow the wear scar to extend continuously into the contact region. Thus, wear continues indefinitely, and extensive damage or catastrophic failure is to be anticipated, given a sufficient number of fretting cycles.

In the elastic régime, the results can be cast in dimensionless terms, permitting application to any material or loading condition. Plasticity introduces an additional dimensionless parameter into the analysis, but results of considerable generality can still be obtained. In particular, the contact pressure distribution exhibits a stable maximum related to the yield strength of the material, and the maximum accumulated plastic strain increases approximately linearly with the number of loading cycles and occurs close to the instantaneous slip-stick boundary.

© 2016 Elsevier Ltd. All rights reserved.

1. Introduction

Partial slip or 'microslip', a common phenomenon in many engineering applications (Ciavarella, 1998a; 1998b; Fouvry et al., 2002; Vingsbo and Söderberg, 1988), occurs when the shear load is insufficient to cause slip throughout a contact interface between deformable bodies. In 'incomplete' or non-conforming contact problems, such as indentation of a plane surface by a cylinder or a punch with rounded edges, the normal tractions decrease smoothly to zero at the contact edge (Ciavarella et al., 1998). However, when the contact is subjected to a cyclic shear load, regions of reversed microslip are developed at the edges of the contact area and the resulting wear leads to a redistribution of stress (Ding et al., 2004; Goryacheva et al., 2001; Johansson, 1994; Kasarekar et al., 2007).

(Hills and Fellows, 1999) showed that the boundary between stick and slip regions does not change during this wear process. This result can be proved rigorously for any problem to which the Ciavarella–Jäger theorem (Ciavarella, 1998a; Jäger, 1998) applies and is also observed in numerical solutions (Ding et al., 2004; Johansson, 1994; Madge et al., 2007). Under these conditions, wear will eventually progress to the state where the contact pressures are negligible in the slip region. Wear will then cease and the system becomes elastically similar to a crack, with consequent square-root singularities in the normal and shear tractions in the stick region, as shown in Fig. 1.

In most practical cases, this process will be limited by plastic deformation near the incipient crack tip, and this in turn may affect the wear process and the evolution of contact pressure. This is the effect to be explored in the present paper. It has potentially important consequences for the prediction of the initiation and propagation of fretting fatigue cracks (Araújo et al., 2006; Fouvry et al., 2002; Giannakopoulos et al., 2000; Kuno et al., 1989; Sum et al., 2005; Vingsbo and Söderberg, 1988).

In many contact systems, the intention is to provide sufficient normal force to approximate a completely stuck situation, so that the resulting cyclic slip zones are small. In particular, if these zones are sufficiently small compared with the other linear dimensions of the problem, the local stress fields can be completely characterized in terms of appropriate generalized stress-intensity factors

---

* Corresponding author. Tel.: +1 7349360406; fax: +1 7346156647.
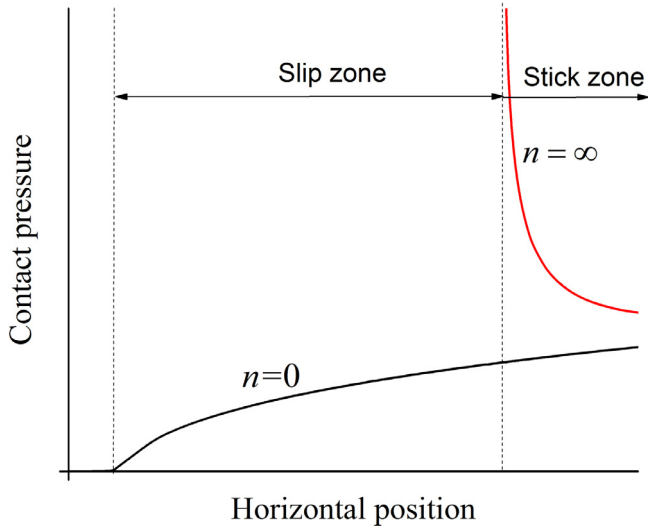E-mail address: jbarber@umich.edu (J.R. Barber).

Fig. 1. The initial contact pressure decreases to zero smoothly. However, after a large number n of loading cycles, the material in the slip zone is worn away and the contact pressure near the stick slip boundary becomes elastically singular.
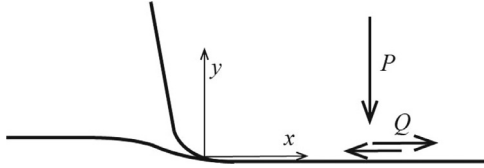

Fig. 2. A contact pair with a smooth contact edge. The indenter is subjected to a normal force P and oscillating force Q. The coordinate x is measured from the edge of the contact.

(Dini and Hills, 2004). This procedure is similar in concept to the 'small-scale yielding' criterion in linear elastic fracture mechanics (LEFM) (Rice, 1974) and has been shown to be very successful in correlating fretting fatigue life (Hills et al., 2012).

In the present paper, we shall use this characterization in the context of a finite-element model to make fairly general predictions about the effect of plastic deformation on the evolution of wear and contact tractions, and on the accumulation of plastic strain during fretting.

2. Methodology

Fig. 2 shows the edge of the contact between two smooth bodies subjected to a constant normal force P and a tangential force that oscillates between $\pm Q$, where $Q < \mu P$ and μ is the coefficient of friction, which is assumed to be the same under static and dynamic conditions. We assume that the line of action of the tangential force lies at the contact interface, so that no moment is induced. We also assume that the materials of the two bodies are similar, so that the second Dundurs' constant, β, is zero (Dundurs, 1969), and hence the slip displacements have no effect on the distribution of contact pressure. This also implies that the critical coefficient of friction defined by Klarbring's 'P-matrix' condition is infinite (Klarbring, 1999), and hence that the incremental frictional problem is well-posed for all values of μ.

2.1. Asymptotic elastic fields

Following Dini and Hills (2004), we characterize the normal tractions local to the contact edge in the absence of wear by the expression

$$p(x) = C\sqrt{x}, \tag{1}$$

where C is a constant that depends on the external loads and the macroscopic geometry. If the length d of the slip zone is sufficiently small compared with the macroscopic length dimensions, the local tangential tractions can then be written as

$$q(x) = \pm\mu C(\sqrt{x} - \sqrt{x - d}) \tag{2}$$

(Dini and Hills, 2004), where the sign depends on the direction of slip and the square roots are interpreted as zero in any region where their arguments are negative.

We assume that the slip zone length d is sufficiently small that there exists a range in which $x \gg d$, but $x \ll D$, where D is a characteristic dimension of the macroscopic contact problem. For practical geometries, this requires that the oscillatory term in the tangential force be much less than the value required for full slip − i.e. $Q \ll \mu P$. However, in the numerical study described in Section 4.1 below, we found that the asymptotic characterization gave predictions within $\pm 3\%$ for values up to $Q = 0.25\,\mu P$. The slip zone has little effect on the shear tractions in $x \gg d$, so these can be characterized by a mode-II stress-intensity factor K_{II} (Ciavarella et al., 1998; Ciavarella and Macina, 2003; Dini and Hills, 2004; Giannakopoulos et al., 2000), where

$$q(x) = \frac{\mu d C}{2\sqrt{x}} = \frac{K_{\mathrm{II}}}{\sqrt{x}}. \tag{3}$$

Notice that this definition differs by a numerical factor of $\sqrt{2\pi}$ from that conventionally used in fracture mechanics.

The parameters C and K_{II} are determined only by the macroscopic geometry and the external loading, and hence could be determined from a numerical model of the system under 'full stick' conditions. Eq. (3) then provides a condition

$$d = \frac{2K_{\mathrm{II}}}{\mu C} \tag{4}$$

for the length of the slip zone, and hence for the local shear traction distribution, through Eq. (2). Notice that this implies the existence of an edge slip zone for all finite values of the coefficient of friction μ, in contrast to 'complete' contact problems, which always stick in the corner if μ is sufficiently high (Churchman and Hills, 2006). Eq. (4) can be used to define a dimensionless coordinate $\xi = x/d$ and a corresponding normalization for tractions can be defined as $\tilde{p} = p/\sigma_0, \tilde{q} = q/\sigma_0$, where the stress measure

$$\sigma_0 = \sqrt{\frac{2K_{\mathrm{II}}C}{\mu}}. \tag{5}$$

With this normalization, all elastic problems are condensed into a single problem, subject only to the 'small slip zone' approximation.

2.2. Effect of wear

Ciavarella (1998a) and Jäger (1998) have shown that when an elastic contact is loaded first by a normal load P and then by a tangential load Q, the stick region $\mathcal{A}_{\mathrm{stick}}$ is coextensive with the contact region $\mathcal{A}^*$ for a fictitious normal load P^* given by

$$P^* = P - \frac{Q}{\mu}. \tag{6}$$

This result also applies at the extreme points where the tangential load is $\pm Q$, during completely reversed periodic loading.

It follows that $\mathcal{A}_{\mathrm{stick}}$ depends only on the profile of the contacting bodies inside $\mathcal{A}_{\mathrm{stick}}$, and this cannot be affected by wear, since wear occurs only where there is slip. Thus, the extent of the stick region remains unchanged throughout the process (Goryacheva et al., 2001; Hills and Fellows, 1999). By contrast, material is worn away in the slip region and eventually, if the process is not limited by yielding, the entire load P will be carried by the stick region. The pressure distribution in this limiting state will comprise the
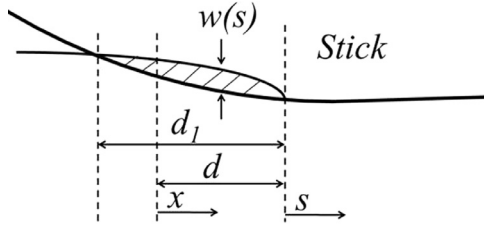
Fig. 3. Overlapping material (shaded) that must be removed in the limiting state.

superposition of (i) $p^*(x)$ due to the fictitious load P^* and (ii) a 'flat punch' distribution due to the additional load $(P - P^*) = Q/\mu$ transferred to $\mathcal{A}_{\text{stick}}$ from the worn region. This latter contribution will lead to a singular traction at the edge of the stick zone, whose magnitude can be characterized by a mode-I stress-intensity factor K_I. Furthermore, since the Green's functions for normal and tangential loading of the half plane are identical in form, Eq. (6) implies that

$$K_I = \frac{K_{II}}{\mu} . \tag{7}$$

2.3. The limiting wear profile

In order to reach this limiting state, material must have been worn from the slip region, corresponding to the overlap that would be implied by the limiting solution if there had been no wear and interpenetration of the bodies had been permitted.

This situation is illustrated in Fig. 3, where the origin of coordinate s is now taken at the edge of the stick region, so $s = x - d$. For $s > 0$, the asymptotic form of the contact pressure is

$$p(s) = \frac{K_I}{\sqrt{s}} + C\sqrt{s} . \tag{8}$$

Near $s = 0$ this expression is consistent with the elastic field around a crack tip with a compressive stress-intensity factor given by Eq. (7), whilst further from $s = 0$ the contact pressure approaches the asymptotic form (1). Note that the parameter C defining the strength of the bounded term is not significantly changed between loads P and P^* as long as the slip zone is sufficiently small.

Application of Williams' asymptotic technique to these fields, shows that the necessary wear $w_\infty(s)$ in $s < 0$ to avoid interpenetration is

$$w_\infty(s) = \frac{4K_I(-s)^{1/2}}{E^*} - \frac{4C(-s)^{3/2}}{3E^*} = \frac{4K_{II}(-s)^{1/2}}{\mu E^*} - \frac{4C(-s)^{3/2}}{3E^*} , \tag{9}$$

where E^* is the composite modulus (Johnson, 1985), which for similar materials is

$$E^* = \frac{E}{2(1 - \nu^2)} , \tag{10}$$

where E and ν are respectively Young's modulus and Poisson's ratio.

Eq. (9) shows that $w(s)$ is positive in a region of length

$$d_1 = \frac{3K_{II}}{\mu C} , \tag{11}$$

and this is exactly 50% larger than the original slip length d from Eq. (4). In other words, as wear occurs, the bodies move closer together, so that the contact region grows. The limiting wear profile (9) can be written in terms of the coordinate $x = s + d$ of Fig. 3 as

$$\widetilde{w}_\infty \equiv \frac{E^* w_\infty}{\sigma_0 d} = 2(1 - \xi)^{1/2} - \frac{4}{3}(1 - \xi)^{3/2} ; \quad -\frac{1}{2} < \xi < 1 , \tag{12}$$

where σ_0 is defined in (5) and we recall that $\xi = x/d$. No wear occurs outside this range.

2.4. Wear model

We assume that wear is governed by the Archard wear law (Archard, 1953) in the form that wear is proportional to the work done against friction. Since the contact pressure is independent of slip displacements, it is approximately constant throughout a single loading cycle, so the wear depth accumulated during the ith loading cycle can be written

$$w_i(x) = 2\mu\alpha p_i(x)\Delta(x) \tag{13}$$

where α is the wear coefficient and $\Delta(x)$ is the local slip displacement during tangential loading from $-Q$ to Q. We can also write this equation in the dimensionless form

$$\widetilde{w}_i(\xi) = \frac{E^* w_i}{\sigma_0 d} = 2\widetilde{\alpha}\,\widetilde{p}_i(\xi)\widetilde{\Delta}(\xi) , \tag{14}$$

where

$$\widetilde{\alpha} = \mu^2 \sigma_0 \alpha ; \quad \widetilde{p}_i = \frac{p_i}{\sigma_0} ; \quad \widetilde{\Delta} = \frac{E^* \Delta}{\mu \sigma_0 d} . \tag{15}$$

With this formulation, wear rates of the order $\widetilde{\alpha} \approx 1$ would cause the steady state $\widetilde{w}_\infty(\xi)$ to be closely approached in a few cycles. Realistic dimensionless wear rates are significantly lower than unity, and indeed must be of order $\widetilde{\alpha} \approx 10^{-2}$ or below for the assumption of constant pressure during each separate cycle to be reasonable.

3. Finite element simulation

In order to determine the effect of wear on the contact stresses, particularly in the presence of yielding, we created a plane-strain, finite-element model in ABAQUS, of the form shown in Fig. 4.

In the system illustrated, microslip and wear will occur at both the left and right edges of the contact area. However, if the microslip regions are sufficiently small compared with the total contact area, they will not interact and it is sufficient to focus attention on the left edge, since with completely reversed loading $\pm Q$, the evolution of wear at the two edges is similar. Very considerable mesh refinement was used in this region, as shown in the two successive insets. The two bodies were modeled by semicircles in order to facilitate appropriate mesh gradation away from the contact region. The contact surfaces were chosen to be circular of large radius, in order that the model could be validated using theoretical results. However, we emphasize that although the model approximates Hertzian contact, the normalization introduced in Section 2 implies that the conclusions are applicable to any problem having a smooth transition from contact to separation.

Sinusoidal tractions $p_b(\theta, \tau)$ were applied at the semicircular boundaries $r = b$ in order to ensure the transmission of the desired forces $P, Q(\tau)$ across the interface. Here, τ is a time-like parameter which is introduced solely in order to define the sequence of loading, since this is periodic and hence non-monotonic. All the results were obtained under quasi-static assumptions and, hence, are independent of loading rate. The model was constrained against rigid body motion by fixing both degrees-of-freedom at one interior node and one degree-of-freedom at another node. It was verified that no unwanted nodal forces were generated at these constrained nodes.

The model was validated by comparing the normal tractions with the classical Hertzian solution, and the shear tractions with the Cattaneo–Mindlin solution (Johnson, 1985). Also, slip displacements, $\Delta(x)$, during the first cycle were compared with theoretical calculations from Goryacheva et al. (2001). In all cases, excellent agreement was obtained.
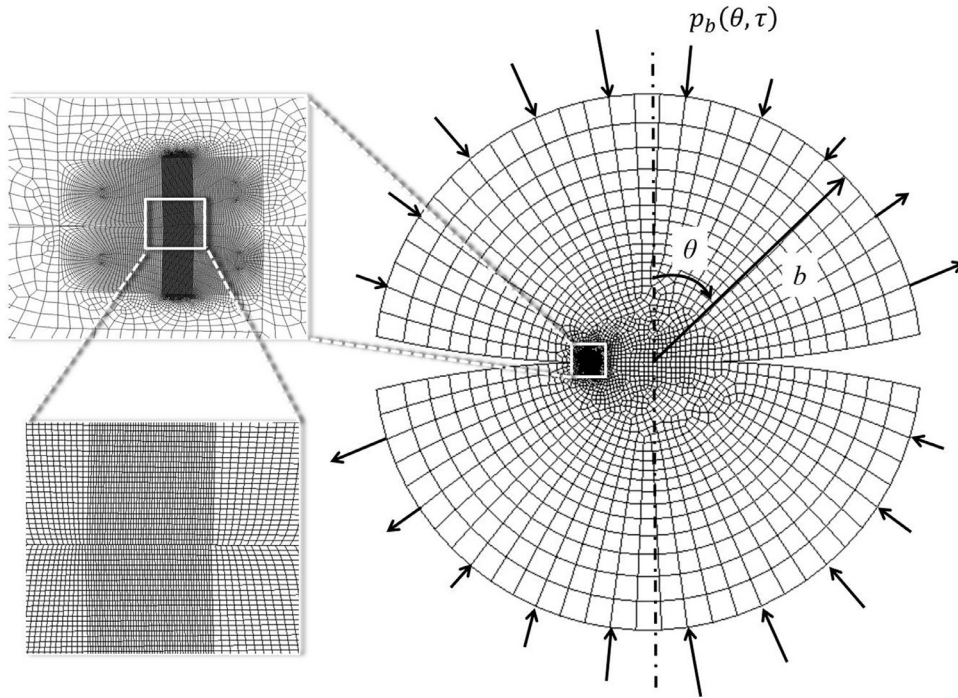
Fig. 4. Finite-element model.

Wear at the slip nodes was calculated using Eq. (14) and the corresponding mesh adjustment was made using the method of fictitious eigenstrains (Hu et al., 2015a). We assume that the worn material is completely removed from the slip zone. In practical situations, the wear process is generally very slow, so that there is very little change in the contact pressure distribution even after hundreds of cycles. For computational efficiency, it is then reasonable to use an enhanced value of $\widetilde{\alpha}$ which is equivalent to considering an appropriate number of successive cycles as having the same pressure distribution.

Various strategies might be used to implement this approximation. Here, we used a linear extrapolation method in which two successive cycles were simulated, including the very small change in the second cycle due to wear, giving values for $\widetilde{w}_i(\xi), \widetilde{w}_{i+1}(\xi)$. The *change* in wear during each of the next n cycles is then assumed to be $[\widetilde{w}_{i+1}(\xi) - \widetilde{w}_i(\xi)]$, so that the total accumulated wear during n cycles is

$$\sum_{j=i}^{i+n} \widetilde{w}_j(\xi) = n\widetilde{w}_i(\xi) + \frac{n(n-1)}{2}[\widetilde{w}_{i+1}(\xi) - \widetilde{w}_i(\xi)] . \qquad (16)$$

4. Results

In this section, we first investigate the evolution of the stress field due to wear under elastic conditions, from which we can determine when yielding is triggered for a given dimensionless yield strength σ_Y/σ_0. We then investigate the subsequent plastic deformation, including its effects on the evolution of the wear profile and the accumulated plastic strain.

4.1. Elastic behavior

As long as the system remains elastic and the slip zone is small compared with the other linear dimensions in the problem, the dimensionless solution is independent of all material and loading parameters, including the coefficient of friction, and a completely general numerical solution can be presented. The evolutionary
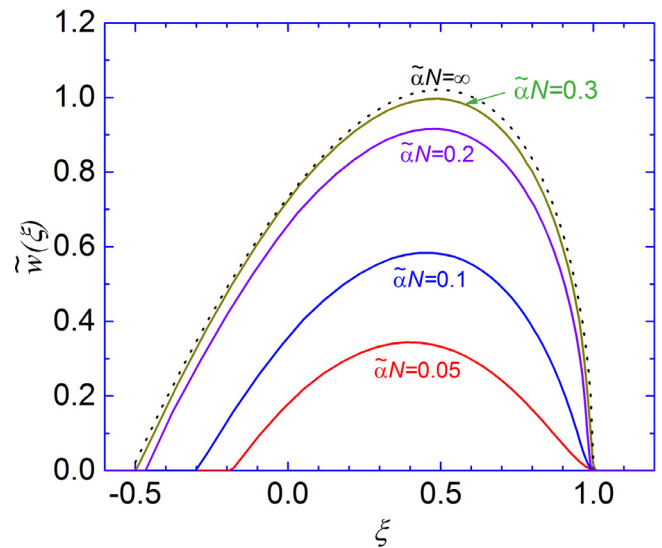

Fig. 5. Evolution of the wear profile with the normalized number of loading cycles $\widetilde{\alpha}N$, from elastic analysis. The dotted curve represents the maximum wear profile in the elastic case, illustrated by the shaded region in Fig. 3 and defined by Eq. (12).

process is then characterized by the product $\widetilde{\alpha}N$, where N is the number of tangential loading cycles. We shall refer to this product as the normalized number of loading cycles.

4.1.1. Wear profile

Fig. 5 shows the dimensionless wear profile $\widetilde{w}(\xi)$ at several values of $\widetilde{\alpha}N$. These results were obtained using a value of n in Eq. (16) corresponding to $\widetilde{\alpha}n \approx 0.16 \times 10^{-3}$. This involved around 1500 applications of the extrapolation strategy of Eq. (16) in the range $0 < \widetilde{\alpha}N < 0.25$, which we found to be more than adequate to achieve numerical convergence. Also, the high degree of mesh refinement ensured extremely smooth results, which are therefore
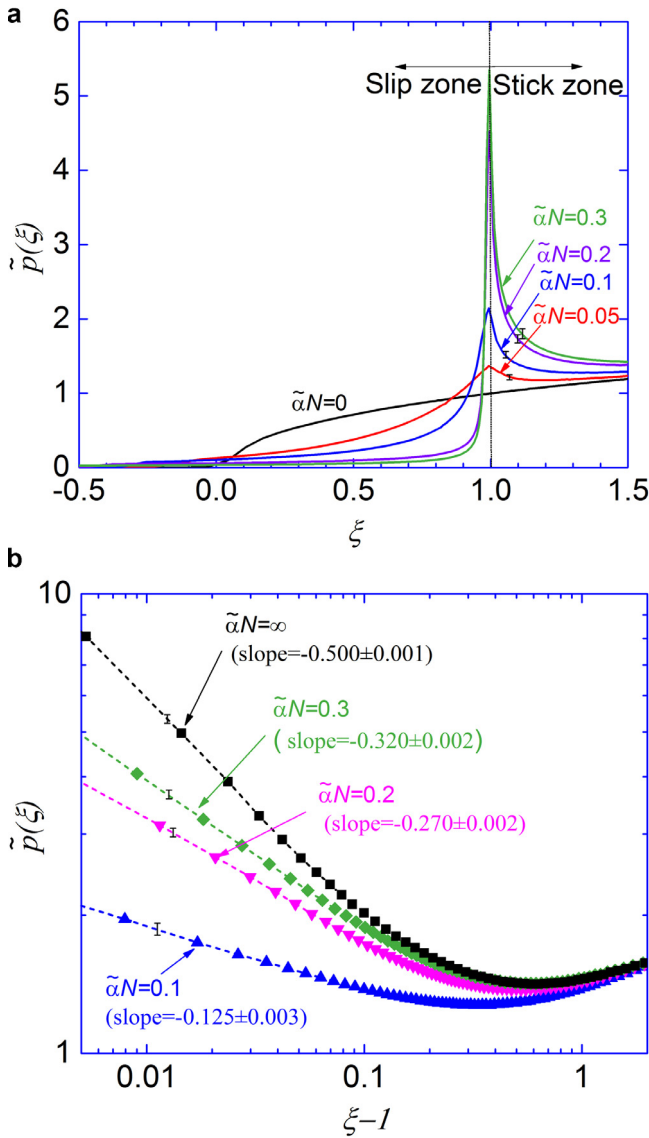
Fig. 7. The maximum von Mises stress associated with the developing contact pressure singularity, from elastic analysis. Notice that early in the wear process, the maximum occurs far from the slip region and is not related to the wear process.

cracks (Sills and Thouless, 2015). Furthermore the peak pressure near the stick-slip boundary $\xi = 1$ continues to grow (without limit) as the wear profile approaches its long-time limit.

4.1.3. Maximum von Mises stress

In real materials, the development of the mode-I singularity at the stick-slip boundary is limited by plastic deformation, which we assume occurs at a critical value, σ_Y, of the von Mises equivalent tensile stress

$$\sigma_e = \sqrt{\frac{3\sigma_{ij}\sigma_{ij} - \sigma_{ii}\sigma_{jj}}{2}} \,. \tag{17}$$

Fig. 7 shows the magnitude of the maximum von Mises stress, $\sigma_e^{\max}$, as a function of $\tilde{\alpha}N$. At the beginning of the process, the maximum occurs far from the slip region, but we obtain an almost linear increase in $\sigma_e^{\max}$ with $\tilde{\alpha}N$ as the peak in contact pressure starts to develop at around $\tilde{\alpha}N \approx 0.1$. The instant at which plastic deformation starts depends, of course, on the ratio σ_Y/σ_0. In all cases, the maximum von Mises stress occurs at the stick-slip boundary on the contact interface.

4.2. Plastic deformation

We next consider the effect of plastic deformation on the evolution of the wear process. We assume that the material is elastic-perfectly plastic, so that yielding occurs at a constant von Mises stress σ_Y. This introduces a new dimensionless parameter σ_Y/σ_0 into the calculation, so we are only able to present particular cases. In order to explore the influence of plastic deformation, we chose the values $\sigma_Y/\sigma_0 = 1$ and 1.5, which we note from Fig. 7 ensure that the contact starts in the elastic régime, but that plastic deformation starts relatively early in the wear process (at $\tilde{\alpha}N = 0.07$ for $\sigma_Y/\sigma_0 = 1$).

4.2.1. Wear profile

Fig. 8 (a,b) shows the development of the wear profile for $\sigma_Y/\sigma_0 = 1$ and 1.5 respectively. The limiting value of wear in the elastic case is shown dotted for comparison. It is clear that plastic deformation allows wear to continue indefinitely both in depth and extent. In particular, the slip-stick boundary extends into the original stick zone and the wear scar also extends further into the original separation zone. This is in sharp contrast to the elastic case,

Fig. 6. (a) Evolution of the dimensionless contact pressure $\tilde{p}(\xi)$ with the normalized number of loading cycles $\tilde{\alpha}N$, from elastic analysis. (b) Plots showing how the stress field near the stick-slip boundary evolves to a crack-like inverse-root singularity as wear progresses. $\xi - 1$ represents the normalized distance from the edge of the wear scar.

presented as lines rather than points in this and subsequent figures.

Notice that the wear profile has reached approximately 95% of its steady-state value at $\tilde{\alpha}N = 0.25$. We also note that the left extent of the slip zone moves steadily towards the limiting value $\xi = -1/2$ as wear progresses, but the stick-slip boundary remains unchanged, as predicted by theoretical arguments (Goryacheva et al., 2001; Hills and Fellows, 1999).

4.1.2. Contact pressure

Fig. 6 shows the corresponding evolution of the dimensionless contact pressure distribution $\tilde{p}(\xi)$. A singular field is developed well away from the boundary of the stick zone for $\tilde{\alpha}N > 0.1$. For small amounts of wear, while there is still significant contact across the wear scar, this singular field is not very strong. However, it tends to the expected inverse-square root value when the wear scar has developed to such an extent that it approximates an unbridged crack. In many ways, this is a direct analogue (in compression) of what is seen in tension for lightly and heavily bridged
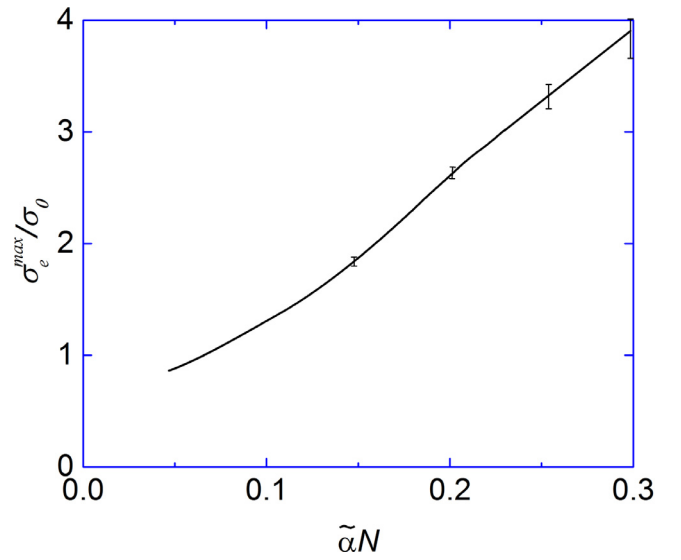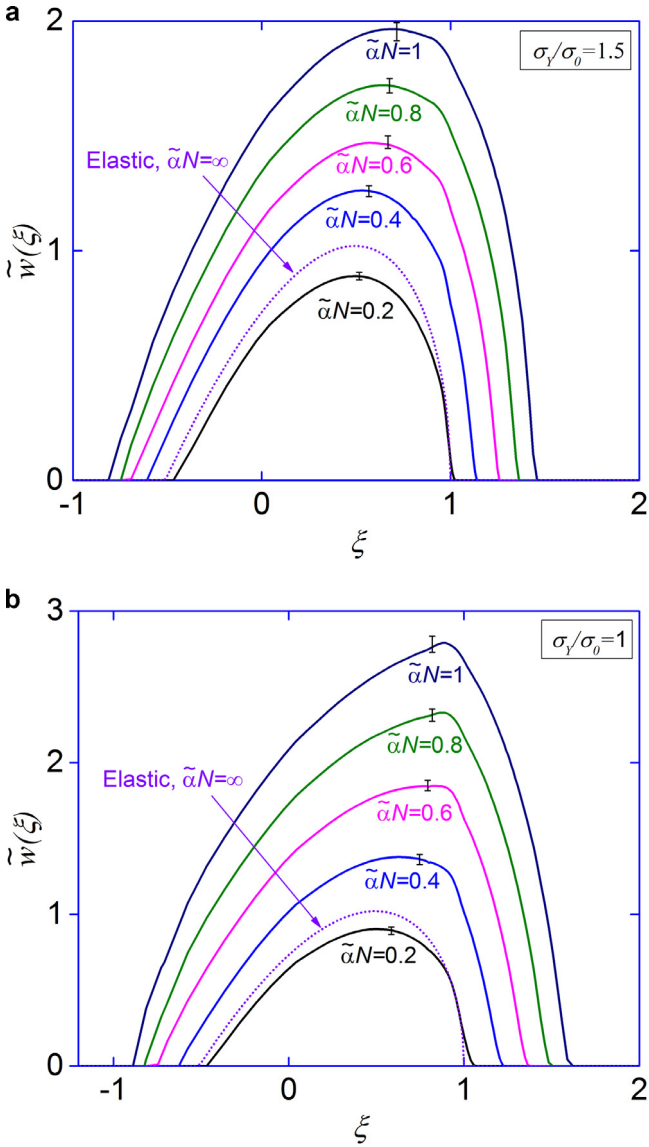
Fig. 8. Development of the dimensionless wear profile $\widetilde{w}(\xi)$ with the normalized number of loading cycles $\widetilde{\alpha}N$ for the elastic-plastic case: (a) $\sigma_Y/\sigma_0 = 1.5$ and (b) $\sigma_Y/\sigma_0 = 1$. The limiting wear in the elastic solution is shown dotted.

Fig. 9. Evolution of the contact pressure distribution $\widetilde{p}(\xi)$ with the normalized number of loading cycles $\widetilde{\alpha}N$ for the elastic-plastic case: (a) $\sigma_Y/\sigma_0 = 1.5$, (b) $\sigma_Y/\sigma_0 = 1$. The dotted curve shows the elastic pressure distribution for $\widetilde{\alpha}N = 0.2$.

where wear is restricted to the original slip zone and is eventually predicted to terminate. The observation that plasticity allows a wear scar to propagate beyond the original stick-slip boundary also applies to situations where the shear stress is limited by the strength of the interface, rather than by plastic deformation in the contacting materials (Hu et al., 2015b). A comparison of Fig. 8(a and b) shows that wear progresses more rapidly when the yield stress is lower.

4.2.2. Contact pressure

The corresponding contact pressure distributions are shown in Fig. 9 (a and b). The most striking feature of these results is that the maximum contact pressure now levels out at about $p_{\max} \approx 2.5\sigma_Y$. This ratio is consistent with values for the maximum normal stress that arise in elastic-plastic crack problems (*e.g.*, Hutchinson, 1968; Tvergaard and Hutchinson, 1992), being slightly less than the limiting value of 2.97 expected from the Prandtl solution for a crack in a rigid-plastic material. The location of this maximum moves to the right as wear progresses, and is always very close to the instantaneous slip-stick boundary.
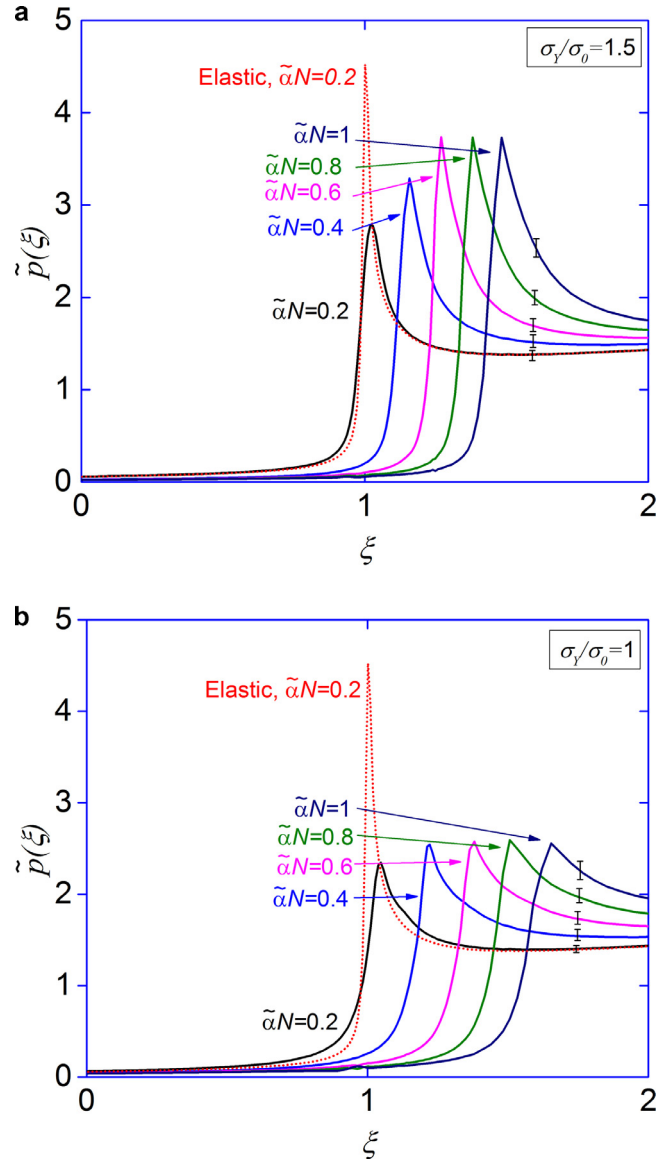
4.2.3. Accumulated plastic strain

As the wear evolves, a plastic zone forms starting from the contact interface and its size grows. The magnitude of the accumulated plastic strain is defined as

$$\varepsilon_e^p = \int_0^\tau \sqrt{\frac{2}{3}\frac{\partial \varepsilon_{ij}^p}{\partial \tau}\frac{\partial \varepsilon_{ij}^p}{\partial \tau}}\, d\tau : \tag{18}$$

where we recall that τ is a time-like parameter characterizing the sequence of loading. The maximum accumulated plastic strain, $\varepsilon_e^{p,\max}$, is considered to be an important indicator of fatigue crack initiation (Abuzaid et al., 2013; Manonukul and Dunne, 2004; McDowell, 2007; McDowell and Dunne, 2010).

Notice that with the definition (18), the plastic strain increases monotonically during cyclic-loading, even if the individual strain components oscillate. Two extreme cases would be (i) if the plastic-strain components reverse completely during each cycle, as in a beam subjected to completely-reversed bending moments, or (ii) if the plastic-strain components accumulate monotonically. Case (i) raises difficulties for the present computational scheme,
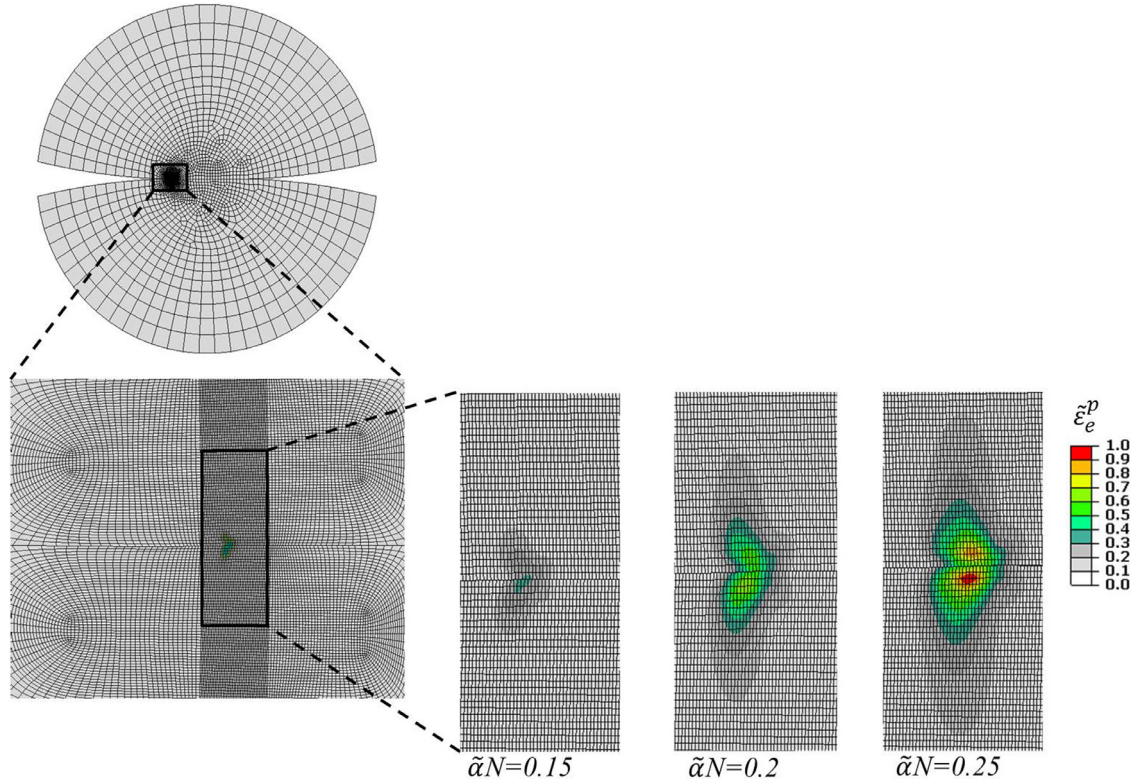
Fig. 10. Contour plot of accumulated plastic strain at three values of $\widetilde{\alpha}N$ ($\sigma_Y/\sigma_0 = 1$).

since it is not practical to simulate every cycle of loading throughout a realistic wear process. We therefore performed a preliminary study in which we simulated $n = 50$ consecutive cycles in the plastic régime, and compared the resulting accumulated plastic strain with that accumulated during a single cycle with an enhanced wear rate of $\widetilde{\alpha}n$. The results differed by less than 3% and, in fact, the single-cycle strain was the largest. We therefore conclude that the evolving plastic strain is a result of monotonic accommodation to the change of profile associated with wear, rather than a result of cyclic plasticity. This also implies that estimates based on a reduced number of cycles with an enhanced wear rate are likely to give good predictions for the accumulation of plastic strain.

Fig. 10 shows contour plots of ε_e^p at $\widetilde{\alpha}N = 0.15$, 0.2, and 0.25 for $\sigma_Y/\sigma_0 = 1$. In the interests of generality, we present these results in the combination

$$\widetilde{\varepsilon}_e^p \equiv \frac{E^* \varepsilon_e^p}{\sigma_0} , \qquad (19)$$

since the results then apply to all systems with the same ratio σ_Y/σ_0. The plastic zone first grows along the contact interface and then spreads in the perpendicular direction. However, the maximum accumulated plastic strain is always located close to the contact interface, and it moves with the slip-stick boundary.

Fig. 11 shows $\widetilde{\varepsilon}_e^{p,\max}$ as a function of $\widetilde{\alpha}N$ for $\sigma_Y/\sigma_0 = 1$ and 1.5. In each case, plastic deformation starts at the value of $\widetilde{\alpha}N$ determined by the appropriate intercept in Fig. 7, and $\widetilde{\varepsilon}_e^{p,\max}$ increases approximately linearly thereafter. It is interesting to note that for higher yield stress, plasticity is delayed, but the plastic strain then accumulates more rapidly. Fig. 11 is terminated at $\widetilde{\alpha}N = 0.3$ because, beyond that point, the plastic zone extends into a region of coarser mesh, implying less accuracy. However, the indications from these less precise calculations are that $\widetilde{\varepsilon}_e^{p,\max}$ continues to increase linearly indefinitely as the wear scar continues to extend.
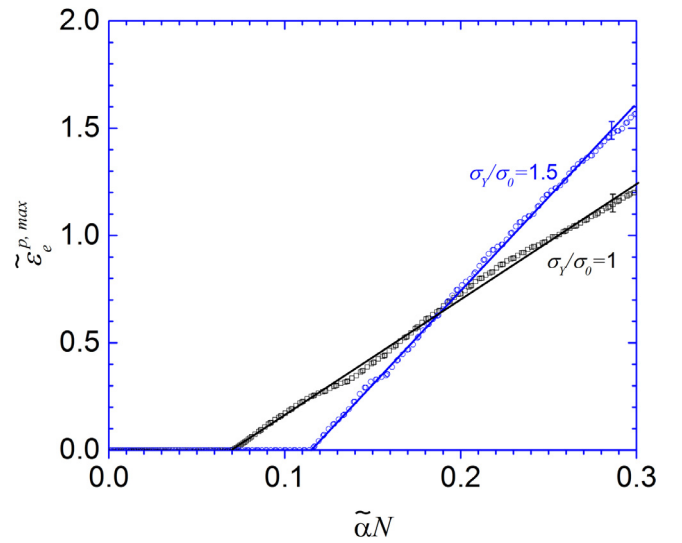

Fig. 11. Maximum accumulated plastic strain $\widetilde{\varepsilon}_e^{p,\max}$ as a function of $\widetilde{\alpha}N$ for $\sigma_Y/\sigma_0 = 1$ and 1.5.

5. Conclusions

We have presented a finite element model of the evolution of local stress fields due to fretting wear, in the case where the normal contact force is constant and the slip zone is small compared with the other linear dimensions of the system. In this limit, the elastic solution characterizes all possible problems of this class. As wear progresses, the slip-stick boundary remains stationary, and the contact pressure distribution develops a local maximum. Eventually, all wear ceases, and the local stress field is characterized by a stress-intensity factor $K_{\mathrm{I}} = K_{\mathrm{II}}/\mu$, where K_{II} is the mode-II stress-

intensity factor for the 'full stick' solution and μ is the coefficient of friction.

By contrast, for elastic-plastic material behavior, the slip-stick boundary moves steadily into the stick region once the yield stress is locally exceeded, and wear continues indefinitely, leading eventually to extensive wear damage. The contact pressure distribution achieves a stable peak value which moves with the slip-stick boundary. Plastic strain accumulates with a maximum at or near this moving boundary, and the maximum accumulated plastic strain increases approximately linearly with subsequent cycles.

Acknowledgments

References

Abuzaid, W., Sehitoglu, H., Lambros, J., 2013. Plastic strain localization and fatigue micro-crack formation in hastelloy x. Mater. Sci. Eng. A-Struct. 561 (0), 507–519.

Araújo, J.A., Vivacqua, R.C., da Silva Bernardo, A.T., Mamiya, E.N., 2006. A crack initiation threshold methodology in fretting fatigue. J. Strain Anal. 41 (5), 363–368.

Archard, J.F., 1953. Contact and rubbing of flat surfaces. J. Appl. Phys. 24 (8), 981–988.

Churchman, C.M., Hills, D.A., 2006. General results for complete contacts subject to oscillatory shear. J. Mech. Phys. Solids 54 (6), 1186–1205.

Ciavarella, M., 1998a. The generalized cattaneo partial slip plane contact problem I-Theory. Int. J. Solids Struct. 35 (18), 2349–2362.

Ciavarella, M., 1998b. The generalized cattaneo partial slip plane contact problem. II- examples. Int. J. Solids Struct. 35 (18), 2363–2378.

Ciavarella, M., Hills, D.A., Monno, G., 1998. The influence of rounded edges on indentation by a flat punch. J. Mech. Eng. Sci. 212 (4), 319–327.

Ciavarella, M., Macina, G., 2003. New results for the fretting-induced stress concentration on hertzian and flat rounded contacts. Int. J. Mech. Sci. 45 (3), 449–467.

Ding, J., Leen, S.B., McColl, I.R., 2004. The effect of slip regime on fretting wear-induced stress evolution. Int. J. Fatigue 26 (5), 521–531.

Dini, D., Hills, D.A., 2004. Bounded asymptotic solutions for incomplete contacts in partial slip. Int. J. Solids Struct. 41 (24–25), 7049–7062.

Dundurs, J., 1969. Discussion on "edge bonded dissimilar orthogonal elastic wedges under normal and shear loading" by d. b. bogy. ASME J. Appl. Mech. 36 (13), 650–652.

Fouvry, S., Elleuch, K., Simeon, G., 2002. Prediction of crack nucleation under partial slip fretting conditions. J. Strain Anal. 37 (6), 549–564.

Giannakopoulos, A.E., Lindley, T.C., Suresh, S., Chenut, C., 2000. Similarities of stress concentrations in contact at round punches and fatigue at notches: implications to fretting fatigue crack initiation. Fatigue Fract. Eng. Mater. 23 (7), 561–571.

Goryacheva, I.G., Rajeev, P.T., Farris, T.N., 2001. Wear in partial slip contact. ASME J. Tribol. 123 (4), 848–856.

Hills, D.A., Fellows, L.J., 1999. Some observations on contact problems involving fretting in the presence of wear. Wear 231 (2), 319–324.

Hills, D.A., Thaitirarot, A., Barber, J.R., Dini, D., 2012. Correlation of fretting fatigue experimental results using an asymptotic approach. Int. J. Fatigue 43, 62–75.

Hu, Z., Lu, W., Thouless, M.D., 2015a. Slip and wear at a corner with coulomb friction and an interfacial strength. Wear 338-339, 242–251.

Hu, Z., Lu, W., Thouless, M.D., Barber, J.R., 2015b. Simulation of wear evolution using fictitious eigenstrains. Tribol. Int. 82 (Part A), 191–194. doi:10.1016/j.triboint.2014.10.015.

Hutchinson, J.W., 1968. Plastic stress and strain fields at a crack tip. J. Mech. Phys. Solids 16, 337–347.

Jäger, J., 1998. A new principle in contact mechanics. ASME J.Tribol. 120 (4), 677–684.

Johansson, L., 1994. Numerical simulation of contact pressure evolution in fretting. ASME J. Tribol. 116 (2), 247–254.

Johnson, K.L., 1985. Contact Mechanics. Cambridge University Press, Cambridge, UK.

Kasarekar, A.T., Bolander, N.W., Sadeghi, F., Tseregounis, S., 2007. Modeling of fretting wear evolution in rough circular contacts in partial slip. Int. J. Mech. Sci. 49 (6), 690–703.

Klarbring, A., 1999. Contact, friction, discrete mechanical structures and discrete frictional systems and mathematical programming. In: Wriggers, P., Panagiotopoulos, P. (Eds.), New developments in contact problems. Springer, Wien, Austria, pp. 55–100.

Kuno, M., Waterhouse, R.B., Nowell, D., Hills, D.A., 1989. Initiation and growth of fretting fatigue cracks in the partial slip regime. Fatigue Fract. Eng. Mater. Struct. 12 (5), 387–398.

Madge, J.J., Leen, S.B., McColl, I.R., Shipway, P.H., 2007. Contact-evolution based prediction of fretting fatigue life: effect of slip amplitude. Wear 262 (9–10), 1159–1170.

Manonukul, A., Dunne, F.P.E., 2004. High- and low-cycle fatigue crack initiation using polycrystal plasticity. Proc. Roy. Soc. (London), A 460, 1881–1903.

McDowell, D.L., 2007. Simulation-based strategies for microstructure-sensitive fatigue modeling. Mater. Sci. Eng. A 468–470, 4–14.

McDowell, D.L., Dunne, F.P.E., 2010. Microstructure-sensitive computational modeling of fatigue crack formation. Int. J. Fatigue 32 (9), 1521–1542.

Rice, J.R., 1974. Limitations to the small scale yielding approximation for crack tip plasticity. J. Mech. Phys. Solids 22 (1), 17–26.

Sills, R.B., Thouless, M.D., 2015. Cohesive-length scales for damage and toughening mechanisms. Int. J. Solids Struct. 55, 32–43.

Sum, W.S., Williams, E.J., Leen, S.B., 2005. Finite element, critical-plane, fatigue life prediction of simple and complex contact configurations. Int. J. Fatigue 27 (4), 403–416.

Tvergaard, V., Hutchinson, J.W., 1992. The relation between crack growth resistance and fracture process parameters in elastic-plastic solids. J. Mech. Phys. Solids 40 (6), 1377–1397.

Vingsbo, O., Söderberg, S., 1988. On fretting maps. Wear 126 (2), 131–147.